



ISTITUTO NAZIONALE DI RICERCA METROLOGICA Repository Istituzionale

Thermodynamics of the Heat-Flux Avalanches at the First-Order Magnetic Transition in Magnetocaloric Materials

This is the author's submitted version of the contribution published as:

Original

Thermodynamics of the Heat-Flux Avalanches at the First-Order Magnetic Transition in Magnetocaloric Materials / Piazzì, Marco; Bennati, Cecilia; Basso, Vittorio. - In: PHYSICAL REVIEW APPLIED. - ISSN 2331-7019. - 8:4(2017). [10.1103/PhysRevApplied.8.044023]

Availability:

This version is available at: 11696/56913 since: 2021-03-02T16:54:29Z

Publisher:

APS

Published

DOI:10.1103/PhysRevApplied.8.044023

Terms of use:

This article is made available under terms and conditions as specified in the corresponding bibliographic description in the repository

Publisher copyright

American Physical Society (APS)

Copyright © American Physical Society (APS)

(Article begins on next page)

Thermodynamics of the heat flux avalanches at the first order magnetic transition in magnetocaloric materials

Marco Piazzai,^{1,*} Cecilia Bennati,² and Vittorio Basso¹

¹*Istituto Nazionale di Ricerca Metrologica, Strada delle Cacce 91, I-10135 Torino, Italy*

²*Istituto dei Materiali per l'Elettronica ed il Magnetismo – Consiglio Nazionale delle Ricerche, Parco Area delle Scienze 37/A, I-43124 Parma, Italy*

We investigate the kinetics of first order magnetic phase transitions by measuring and modelling the heat flux avalanches corresponding to the irreversible motion of the phase boundary interface separating the coexisting low- and high-temperature stable magnetic phases. By means of out-of-equilibrium thermodynamics we encompass the damping mechanisms of the boundary motion in a phenomenological parameter α_s . By analyzing the time behaviour of the heat flux signals measured on $\text{La}(\text{Fe-Mn-Si})_{13}\text{-H}$ magnetocaloric compounds through Peltier calorimetry temperature scans performed at low rates, we relate the linear rise of the individual avalanches to an intrinsic thermal resistance associated to α_s .

PACS numbers: 75.30.Sg, 05.70.Ln, 64.70.K-

Keywords: magnetocaloric effect; first order transitions; out-of-equilibrium thermodynamics

I. INTRODUCTION

Magnetic refrigeration around room temperature is emerging as an environmental-friendly, efficient and increasingly feasible alternative to the conventional vapour-compression cooling technology^{1–5}. The physical effect underlying this technique is the magnetocaloric effect (MCE), corresponding to the magnetic field induced isothermal entropy change $\Delta S_{\text{iso}}(H)$ and the adiabatic temperature change $\Delta T_{\text{ad}}(H)$ occurring in magnetically ordered solid materials under a varying applied magnetic field H ^{6,7}. Recently, many results have been achieved in the search for materials showing optimal properties for applications, e.g. first order magnetostructural transitions finely tunable around room temperature, low thermal hysteresis, high entropy and temperature changes^{8–13}. Nevertheless, the practical realization of cooling engines based on active magnetic regenerative refrigeration (AMRR) cycles still suffers from some open issues, mainly dealing with the operation frequency of the devices. Although the design of such devices has been substantially improved by the contributions and proposals of many different research groups^{14–32}, the operation frequency of AMRR-based engines has been only partially worked out. In Ref. [33], Kuz'min has shown that this frequency depends on the characteristic relaxation time constants related to the thermal conductivity of the solid refrigerant (τ_{tc}), to the viscosity of the heat-exchange fluid (τ_{fc}) and to the magnetic processes occurring in the MCE material during the AMRR cycles (τ_{mr}). The conditions to reduce both τ_{tc} and τ_{fc} , relating them to the values of two parameters, d_r and d_f , representing the cross sections of the refrigerator channels filled with the MCE material and the heat-exchange fluid, respectively, are known³³. However, the intrinsic magnetic relaxation process has been neglected, assuming that the MCE material magnetizes or demagnetizes itself instantaneously when the applied magnetic field is switched on or off. While this can be valid for materials

undergoing second order transitions³⁴, it is known that this is not usually the case when dealing with first order ones^{35–47}. In this case both the microscopic domain nucleation events, driven by the defects present in the material, and some extrinsic factors limit the kinetics of the magnetization or demagnetization processes. Many efforts have been done trying to clearly distinguish the contributions of these different effects. In particular, it has been shown that a viable route in this direction is represented by the development of experiments in which the MCE properties of the materials are measured by varying the magnetic fields at a high sweep rate of about 10–100 Hz, representing the typical working frequencies of magnetic cooling devices^{48–50}.

By performing magnetic measurements at different field-rates on $\text{La}(\text{Fe-Si})_{13}$ samples, Moore et al.³⁵ and Lovell et al.³⁹ have indeed succeeded in separating the intrinsic and extrinsic factors contributing to the specific heat of a MCE system. They have shown that the use of magnetic fields varying in time at a fast enough rate, i.e. $\gtrsim 5 \text{ mT/s}$ corresponding to a cycling frequency of about 10^{-2} Hz/T , allows to determine how the MCE properties of the system are affected by three major factors, namely the geometrical properties of the MCE sample, the heat diffusion processes occurring into the system and finally the thermal contacts between the sample and the measuring setup. However, a detailed quantitative analysis of the intrinsic contributions to the transition kinetics due to the nucleation and growth of a new stable magnetic phase has not been performed.

Such an analysis has been instead reported in Ref. [44], where a theoretical approach based on the Johnson-Mehl-Avrami model^{51–54} has been applied to explain the experimental features observed in the magnetic susceptibility of $\text{La}(\text{Fe}_{0.88}\text{Si}_{0.12})_{13}$ compounds. This model relates the kinetics of first order transitions to the dynamics of a thermally activated process, by assuming the existence of a barrier in the energy landscape between the ferro-(FM) and paramagnetic (PM) states, that shall be over-

come through random thermal fluctuations in order to make the transition start. Later on, other authors⁴⁶ have shown that similar experimental results can be attributed also to extrinsic effects, namely the presence of bad thermal contacts between the sample and the external bath. In view of these results, the role played by such extrinsic effects on the model proposed by Yako and Fujita⁴⁴ shall be deeper investigated and better clarified.

A possible step forward on this topic can be done by analyzing the heat flux behaviour obtained through calorimetry scans performed on MCE materials at fixed temperature by changing H at low rate³⁷ or, vice versa, by slowly varying the temperature at fixed H ^{47,55}. It has been shown that the heat flux signal presents sequences of avalanches well separated in time close to the transition temperature. These avalanches vary in shape and number by approaching the critical point (T_c, H_c) of the system and they can be associated to the latent heat of the system^{37,55}. Above the critical point, they essentially disappear leaving only a continuous background associated to the reversible specific heat of the material. The key point to observe is that their time behaviour mirrors the kinetics of the nucleation and pinning processes occurring during the phase transition. However, since the scan rates employed in the experiments are very slow, both intrinsic and extrinsic factors contribute to determine this kind of behaviour.

In this paper we address this issue from a theoretical point of view, by modelling the time behaviour of the heat flux signals experimentally detected through temperature scans performed at 1 mK/s rate and various applied magnetic fields H on a series of $\text{La}(\text{Fe-Mn-Si})_{13}\text{-H}_{1.65}$ compounds. To approach the problem, the thermodynamics of a moving front in a first order phase transformation shall be described, by focusing in particular on the factors limiting its velocity. In the classical Stefan problem^{56–58}, the phase front is described at the equilibrium temperature and the heat diffusion processes limiting its growth are considered. Within this approach, the thermodynamic equilibrium is maintained at the expense of the emergence of strong local temperature gradients. In the present case of solid-solid phase transitions occurring in the MCE materials, we are dealing with metals characterized by a high heat conductivity and a distribution of defects which suggest to use an out-of-equilibrium description of the moving front. In this case, the latter is allowed to be at a temperature different from the equilibrium one⁵⁹ and the temperature gradients will be relevant only on length scales much larger than the microstructural ones. For this reason, we propose a model, based on the out-of-equilibrium theory of linear systems, able to describe both the intrinsic microscopic processes governing the transition and giving rise to the appearance of the latent heat, and the extrinsic contributions due to the thermal contacts. In the paper we show that the intrinsic microscopic processes can be associated to the motion of the phase boundaries interface separating the PM and FM stable phases coexisting during the transition, while

the thermal bath details fully determine the relaxation behaviour of the system back to the thermodynamic equilibrium after the transition is occurred. In particular, the damping mechanisms governing the boundary interface motion and giving rise to the latent heat of the system Δu_L are encompassed in a phenomenological parameter α_s that we evaluate by comparison of the experimental data with the model. Within the uncertainty limits, we find that $\alpha_s/\Delta u_L \approx 0.5 \times 10^{-3} \text{ (m/s)/K}$, independently on both H and the material composition. Moreover, we determine the time scales involved in the transition process, showing that the intrinsic damping and the heat exchange with the external thermal bath are governed by time constants having the same order of magnitude.

The paper is organized as follows. In Sec. II we introduce the out-of-equilibrium thermodynamic theory of linear systems that we have used to describe first order transitions. First we focus on the description of homogeneous systems (Sec. II A), then extending the theory to the case of macroscopic samples in which phase coexistence may arise (Sec. II B) and finally deriving the kinetic constitutive equation of the system by comprising the role of the specific heat due to electrons and phonons (Sec. II C). In Sec. III we apply the above theory to the analysis of solid-state MCE samples in quasi-isothermal conditions by adding the role of an external thermal reservoir (Sec. III A) and we find the theoretical behaviour of the heat flux in the case of individual-avalanche events (Sec. III B). In Sec. IV we compare the theoretical predictions with the experimental data obtained by performing Peltier calorimetry temperature scans at low rate and in Sec. V we discuss the results obtained, suggesting also possible routes for future works. Finally, in Sec. VI we present our conclusions.

II. OUT-OF-EQUILIBRIUM THERMODYNAMICS OF FIRST ORDER PHASE TRANSITIONS

A. Homogeneous systems

Let us consider a magnetic system characterized by the entropy S and the magnetic moment m . Since the controlled magnetic variable is the magnetic field H , we can describe the system through the enthalpy potential $U_e(S, H) = U - \mu_0 H m$, where U is the internal energy⁶⁰. A first order phase transition will be characterized by a non monotonic behaviour of the equation of state

$$T_p(S, H) = \frac{\partial U_e}{\partial S}, \quad (1)$$

so that the temperature of the system T will not follow everywhere the equilibrium temperature path defined by T_p . The typical behaviour is depicted in Fig. 1, where we show the out-of-equilibrium path as $1/T_p$ as a function of the enthalpy U_e . Upon heating, after reaching the limit of stability, i.e. point A in Fig. 1, T will pass through a

sequence of high energy out-of-equilibrium states going towards the first available equilibrium state, i.e. point B in Fig. 1. The rate at which T relaxes towards the new equilibrium state should be determined by means of non equilibrium thermodynamics.

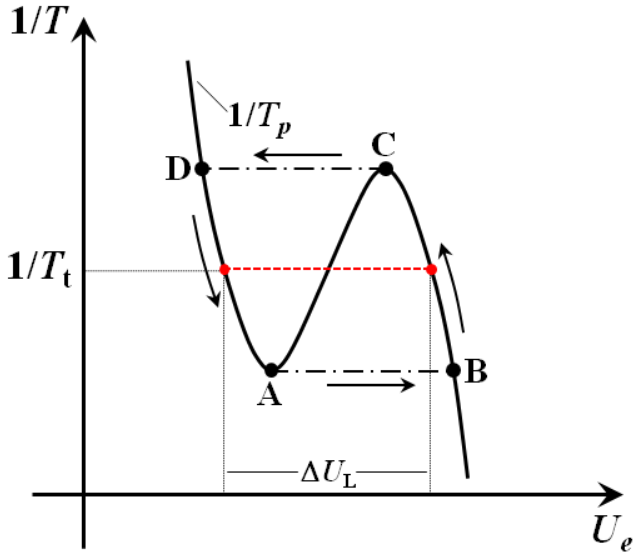


Fig. 1. Out-of-equilibrium first order transition in homogeneous systems: temperature $1/T_p$ (Eq. (1)) vs. enthalpy U_e . Arrows show the path followed by the system upon heating (D-A-B) and subsequent cooling (B-C-D); dash-dotted black lines represent the out-of-equilibrium states explored during the transition, after the limits of stability A and C are overcome. $1/T_t$ (dashed red line) is the equilibrium transition temperature path followed according to the Maxwell construction (see also Fig. 2). ΔU_L is the enthalpy change at T_t , whose volume density Δu_L appears in Eq. (8) and in Table I.

The main observation to take into account is that, when T is in a non equilibrium state higher than T_p (Eq. (1)), the entropy change per unit time dS/dt is $(1/T_p) \partial U_e / \partial t$ which is higher than $(1/T) \partial U_e / \partial t$. The difference is associated to the presence of internal entropy production processes. Therefore, by describing the internal entropy production processes through the entropy production rate $\Sigma_s \geq 0$, the entropy change rate reads:

$$\frac{dS}{dt} = \frac{1}{T} \frac{dU_e}{dt} + \Sigma_s. \quad (2)$$

From Eq.(1) and Eq. (2) we immediately obtain the following expression for the entropy production rate:

$$\Sigma_s = \left(\frac{1}{T_p} - \frac{1}{T} \right) \frac{dU_e}{dt}. \quad (3)$$

In Eq. (3) we can recognize two different terms. The first one, dU_e/dt , represents the velocity of the relaxation process bringing the system temperature T back to the equilibrium value. The second term, $(1/T_p - 1/T)$, is proportional to the distance of the system temperature T from the equilibrium value T_p . Then, in the framework

of out-of-equilibrium thermodynamics of linear systems, the latter term acts as the generalized force responsible for the relaxation process, while the former term is a generalized displacement. When the displacement term is small enough, it is possible to assume that the displacement and the force are linearly coupled and thus the relaxation equation describing the rate at which any generic out-of-equilibrium state reaches the equilibrium one is given by

$$\frac{dU_e}{dt} = \alpha T_p^2 \left(\frac{1}{T_p} - \frac{1}{T} \right), \quad (4)$$

where the proportionality coefficient α has the units W/K.

B. Phase coexistence state

In a macroscopic system composed by many internal and interacting degrees-of-freedom a first order transition may occur differently with respect to what described in the previous section. Indeed, the system may build up a mixture of the low (LT) and high temperature (HT) stable phases, because the phase coexistence may be more favourable from an energetic point of view. In particular, the phase coexistence defines a transition temperature at equilibrium T_t which is obtained by means of the Maxwell construction. This construction consists in replacing the non monotonic part of $T_p(S)$, defined in Eq. (1), with the constant temperature T_t , as shown in Fig. 1 and Fig. 2. The latter is the temperature at which the two minima in the Gibbs free energy representation have the same value, i.e. $G_L(S_0; T_t) = G_L(S_1; T_t)$, where $G_L(S; T) = U_e(S) - TS$ and $S_0(T)$, $S_1(T)$ are the temperature-dependent minima of $G_L(S; T)$, satisfying $\partial G_L / \partial S|_{S=S_0} = \partial G_L / \partial S|_{S=S_1} = 0$. It is worth noting that S_0 and S_1 represent the entropies of the LT and HT stable magnetic phases which coexist at T_t . In particular, from Eq. (1) and from the Maxwell construction, we obtain that the enthalpy change rate at equilibrium and in the phase coexistence region can be expressed as $dU_e/dt = T_t dS/dt$.

However, this equilibrium picture is not always realized. The nucleation and pinning of the individual domains may occur at a sample temperature T different from T_t , because of the local defects present in the material microstructure. This means that when transforming in heating from the LT to the HT, or viceversa in cooling from the HT to the LT phases, a specific nucleation event i will be characterized by a critical value T_{hi} higher, or T_{ci} lower, than T_t (see Fig. 2). Being T different from the equilibrium value T_t , we shall consider also in this case the role of the entropy production processes introduced in Sec. II A. Analogously to Eq. (2), the entropy change rate dS_i/dt associated to the i -th event will be in this case

$$\frac{dS_i}{dt} = \frac{1}{T} \frac{dU_{ei}}{dt} + \Sigma_{si}, \quad (5)$$

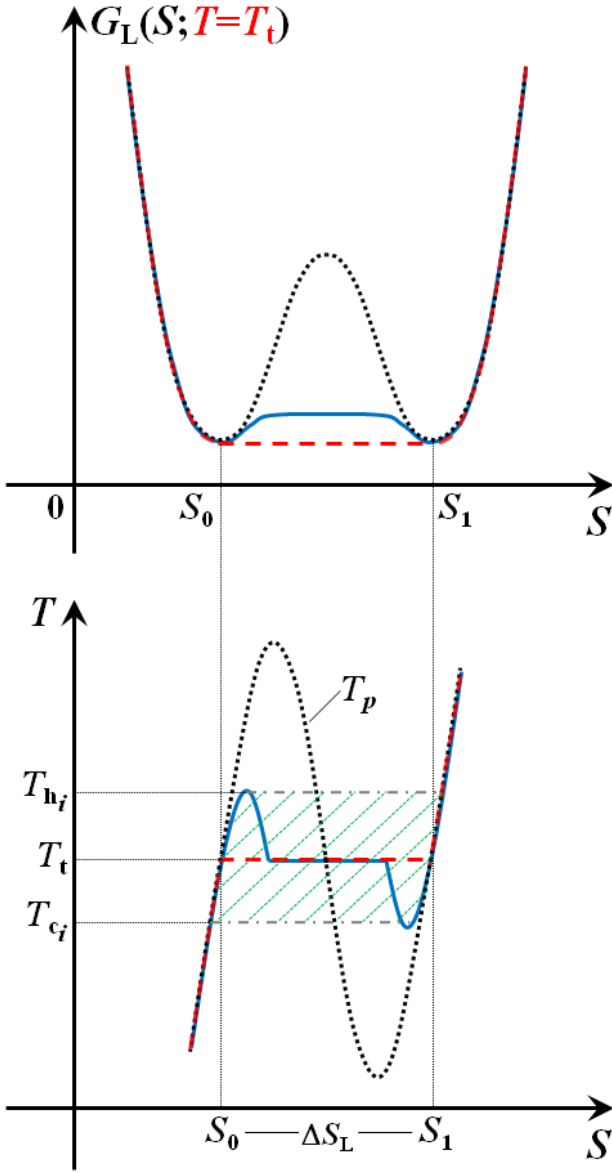


Fig. 2. Gibbs free energy $G_L(S; T = T_t)$ (top) and temperature $T = \partial U_e / \partial S$ (bottom) vs. entropy S , in first order transitions, for: (i) a homogeneous system (black dotted line) in which the transition follows the T_p curve (Eq. (1)); (ii) a macroscopic system (red dashed line) in which the transition occurs through the Maxwell construction at the equilibrium temperature T_t ; (iii) an irreversible domain nucleation event i (pale blue solid line) occurring around a defect at temperature T_{hi} (T_{ci}) upon heating (cooling). Green lines highlight the LT-HT phase coexistence region; $\Delta S_L = S_1 - S_0$ is the entropy change at T_t between the entropies S_0 , S_1 of the LT and HT stable magnetic phases.

so that the entropy production rate will be given by

$$\Sigma_{si} = \left(\frac{1}{T_t} - \frac{1}{T} \right) \frac{dU_{ei}}{dt}. \quad (6)$$

In the latter equation we recognize a velocity term, i.e. dU_{ei}/dt , and a displacement term, i.e. $1/T_t - 1/T$. By

means of the same reasoning developed in Sec. II A to obtain Eq. (4), we end up with the following linear expression for the enthalpy change rate occurring in the phase coexistence region:

$$\frac{dU_e}{dt} = \alpha T_t^2 \left(\frac{1}{T_t} - \frac{1}{T} \right). \quad (7)$$

On the other hand, we can get another expression for the enthalpy change rate dU_e/dt by relating the latter to the microscopic events giving rise to the phase transition. We will assume that the transition is driven by the motion of the phase boundary interface separating the LT and HT magnetic states which is nucleated at the defects present in the material microstructure. This interface can be thought of as a surface of total area A that moves with a certain velocity. If we assume to deal with an ideally thin interface, the phase transformation will be due to the displacement of the position of the interface in time, $x(t)$, and the enthalpy change rate can be expressed as

$$\frac{dU_e}{dt} = \Delta u_L A \frac{dx}{dt} \quad (8)$$

where $\Delta u_L = T_t \Delta s_L > 0$ is the enthalpy change per unit volume at T_t , i.e. the latent heat of the system (see Fig. 1), and Δs_L is the isothermal entropy density change at the transition.

By substituting Eq. (8) into Eq. (7) and by defining the proportionality coefficient $\alpha_s = \alpha/A$, having units $\text{W K}^{-1} \text{m}^{-2}$, we immediately get the following expression for the velocity of the phase boundary interface:

$$\frac{dx}{dt} = \frac{\alpha_s}{\Delta u_L} T_t^2 \left(\frac{1}{T_t} - \frac{1}{T} \right). \quad (9)$$

It is worth noting that Eq. (9), through the coefficient α_s , encompasses the details of the damping mechanisms of the phase boundary motion, thus describing the kinetics of the relaxation processes occurring at first order phase transitions in macroscopic systems. Finally, the expression for the latent heat of the system is

$$\frac{dU_e}{dt} \simeq \alpha_s A (T - T_t), \quad (10)$$

where Eq. (10) is obtained from Eq. (7) and holds only if $T \simeq T_t$.

C. Constitutive kinetic equation for the material

Magnetic phase transitions in solid-state systems are characterized not only by the latent heat (Eq. (10)), but also by electronic and structural reversible contributions to the enthalpy that are proportional to the heat capacity C_s of the region of the sample involved by the phase transformation. The full enthalpy variation is then obtained by simply adding the latent heat contribution and

the reversible one, so that

$$\frac{dU_e}{dt} = C_s \frac{dT}{dt} + \alpha_s A (T - T_t). \quad (11)$$

Here, we further consider that in the sample many irreversible events may occur concurrently, each one of them involving the motion of a portion of the whole phase boundary interface characterized by a surface area A_i , so that $A = \sum_i A_i$. Moreover, it is relevant to introduce the typical linear size λ over which the temperature T is uniform into the sample (see Fig. 3 for a schematic view of the typical length scales involved in the description of the irreversible events occurring in a first order magnetic phase transition).

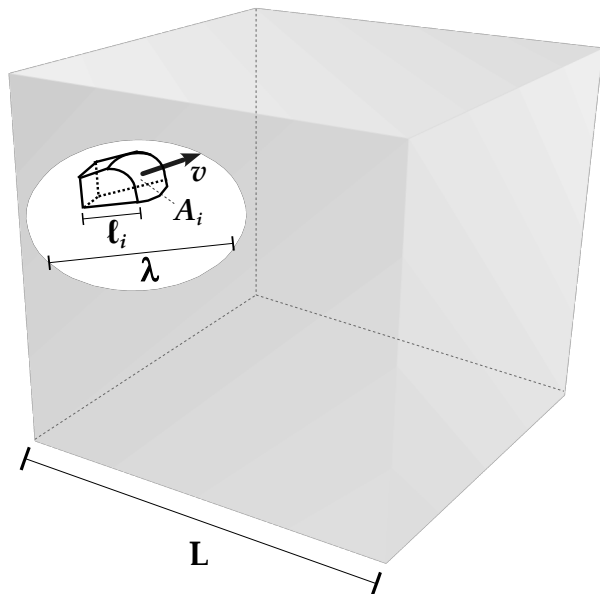


Fig. 3. Typical length scales involved in the irreversible events driving a MCE system through a first order magnetic transition: L is the linear size of the sample, λ represents the linear size of the region in which T is uniform and ℓ is the linear size of the region swept out by the i -th piece of boundary interface of surface area $A_i \sim \ell_i^2$ during its motion at velocity v (see Eq. (9)). The size λ depends on the heat diffusion properties of the system and can be either $\ll L$ for macroscopic samples or $\gtrsim L$ for small fragments; the size ℓ depends instead on the material microstructure and in this work we assume $\ell_i \ll \lambda$.

With the above assumptions, the expression for the specific enthalpy rate becomes

$$\frac{du_e}{dt} = c_s \frac{dT}{dt} + \sum_i \alpha_s \frac{A_i}{\lambda^3} (T - T_t), \quad (12)$$

where $c_s = C_s/\lambda^3$ is the specific heat of the system and $u_e = U_e/\lambda^3$ is the enthalpy normalized to the volume λ^3 . It is worth pointing out that each of the microscopic events i contributing to the sum in Eq. (12) is activated at its own temperature $T_{hi} > T_t$, in an heating process, or $T_{ci} < T_t$ in the cooling case, as already described in

Sec. II B and depicted in Fig. 2. This fact means that the motion of each portion of the boundary surface is activated by overcoming different energy barriers. Then, Eq. (12) shows that the events i within the volume λ^3 are correlated because the activation of a certain single event will cause the decrease, upon heating, or the increase, upon cooling, of the temperature T within the whole volume λ^3 , therefore inhibiting the activation of the other domains motion.

Finally, the enthalpy variation described by Eq. (12) is coupled to the macroscopic heat current density \mathbf{j}_q through the continuity equation

$$\frac{du_e}{dt} + \nabla \cdot \mathbf{j}_q = 0. \quad (13)$$

III. KINETICS OF HEAT FLUX AVALANCHES

A. Kinetics in quasi-isothermal conditions

In order to unveil the local variations of the sample temperature T occurring in a phase transition caused by the presence of a distribution of different activation temperatures T_{ci} , T_{hi} , let us consider to connect the MCE sample to a thermal reservoir having uniform temperature T_b , through a thermal contact. The latter is conveniently represented as a region characterized by a surface area A_c and a thickness t_c . The current density $j_q = \|\mathbf{j}_q\|$ associated to the heat flowing through the contact along the direction orthogonal to the surface A_c is then given by

$$j_q = -\kappa_c \frac{T_b - T}{t_c}, \quad (14)$$

where κ_c is the thermal conductivity of the contact and in the equality we have assumed that the temperature varies linearly inside the contact thickness t_c .

On the other hand, the current density \mathbf{j}_q is also related to the enthalpy change rate du_e/dt through the continuity equation given by Eq. (13). In what follows, we will limit ourselves to investigate the case in which the temperature T can be considered as uniform in the whole sample, so that we can neglect the role of the heat diffusion processes occurring inside the sample itself. This assumption is valid when the macroscopic linear size of the sample L (see Fig. 3) is smaller than λ and the thermal conductivity κ of the MCE material, appearing in the relation $\mathbf{j}_q = -\kappa \nabla T$, is high. With the above assumptions, we can explicitly express the heat current density \mathbf{j}_q as a function of the enthalpy rate du_e/dt by integrating the continuity equation Eq. (13) over the volume λ^3 . Since the surface area through which the heat current flows perpendicularly and which encompasses the integration volume is λ^2 , by means of the divergence theorem we get the result $j_q = -\lambda du_e/dt$. By taking now the latter equation equal to Eq. (14) and by substituting the

enthalpy rate du_e/dt with Eq. (12), we obtain the differential equation governing the time behaviour of $T(t)$ during the phase transition:

$$\begin{aligned} \frac{dT}{dt} &= \frac{\kappa_c}{\lambda c_s t_c} (T_b - T) - \sum_i \frac{\alpha_s A_i}{\lambda^3 c_s} (T - T_i) \\ &= \frac{T_b - T}{\tau_c} - \sum_i \frac{T - T_i}{\tau_{si}}. \end{aligned} \quad (15)$$

In Eq. (15) we have defined the time constants $\tau_c = \lambda c_s t_c / \kappa_c$ and $\tau_{si} = \lambda^3 c_s / (\alpha_s A_i)$. While the latter, through the coefficient α_s and the typical sizes λ and A_i , is related only to the intrinsic kinetics and the damping mechanisms governing the phase transition, the former takes into account the role of the external thermal reservoir through the thermal contact resistance $t_c / (\kappa_c A_c)$.

The solution of Eq. (15) is strictly dependent not only on the initial conditions on T , but also on the time behaviour of the thermal reservoir temperature $T_b(t)$. There are two cases of particular interest: (i) constant T_b ; (ii) T_b varying at constant rate \dot{T}_b . The former condition ensures that the motion of each piece of boundary interface of surface area A_i is separated in time from the other ones. This happens because when the surface A_i starts to move, the temperature T becomes lower than T_{hi} upon heating, or higher than T_{ci} upon cooling, in a volume λ^3 which in our case corresponds to the whole sample, since we are assuming $L < \lambda$, this way inhibiting the occurrence of other events. This case is described in details in the following Sec. IIIB and in Appendix A.

The case of a reservoir temperature T_b varying in time at a constant rate \dot{T}_b is also very interesting from both a physical and a mathematical point of view. Indeed, when T_b varies uniformly in time, many events i , each one corresponding to the motion of a piece of boundary surface A_i , may occur concurrently and collectively contribute to the sum appearing on the right-hand side of Eq. (15). This happens because the heat provided by the thermostat to the MCE sample during the phase transition is enough to overcome the change in temperature occurring within the λ^3 volume. The solution $T(t)$ shows in this case many qualitatively interesting features and it is derived in Appendix B.

B. Individual avalanches

Let us address now the case of a thermal reservoir temperature T_b kept constant in time during the phase transition. Then, as explained in Sec. III A, we can further simplify Eq. (15) because in this case the individual events i , associated to the motion of the portions of boundary interface of surface area A_i , are well separated in time. For the sake of simplicity, we will assume from here on that $A_i \sim \ell_i^2$, meaning that the surface area of each portion of the boundary interface scales as the square of the typical linear size ℓ_i covered by the interface during its motion (see Fig. 3). It is worth noting that

the ℓ_i value is strictly related to the sample microstructure determining the nucleation and pinning centres for the formation of a new phase and we will assume $\ell_i \ll \lambda$. This way, we can consider these events as independent one of each other and we can investigate the effect that each of them, taken one at a time, has on the time evolution of T . This assumption means that the sum appearing in Eq. (15) reduces to only one term and therefore, by defining t_i, t_f as the times at which the event starts and ends, we can conclude that the time behaviour of T during a first order transition driven by a single irreversible event is governed by the following differential equation:

$$\frac{dT}{dt} = \frac{T_b - T}{\tau_c} - \frac{T - T_i}{\tau_{si}} \quad \text{for } t_i \leq t \leq t_f, \quad (16)$$

For $t > t_f$, once the transition is ended, the contribution of the latent heat associated to the boundary motion will not be present anymore in Eq. (12) and the differential equation governing the behaviour of the sample temperature $T(t)$ will be:

$$\frac{dT}{dt} = \frac{T_b - T}{\tau_c} \quad \text{for } t > t_f. \quad (17)$$

It is worth noting that Eq. (16) describes the system during the phase transition, when T varies because of both the effect of the external thermal contacts and of the intrinsic kinetics of the moving boundary interface which absorbs or releases heat, depending on whether we are dealing with an heating or a cooling process, thus reducing or enhancing T with respect to its initial value. On the other hand, Eq. (17) describes the behaviour of the system once the transition is ended and the temperature T relaxes back to the thermodynamic equilibrium value governed only by the heat exchanged with the thermal reservoir.

The solutions of Eqs. (16)–(17) for constant T_b and $t_f - t_i \ll \tau_c, \tau_{si}$ are analytically derived in Appendix A. It is worth pointing out that the condition $t_f - t_i \ll \tau_c, \tau_{si}$ ensures that the sample temperature T , and consequently the heat flux $q_s(t)$, are far from the thermodynamic equilibrium during the whole phase transition and that the transformation will thus occur through a sequence of out-of-equilibrium states far from T_i (see also Fig. 2). In particular, the time behaviour of the heat flux $q_{si}(t)$ for an individual avalanche is given by:

$$q_{si}(t) = \begin{cases} \pm \frac{\lambda^3 c_s}{\tau_c \tau_{si}} \frac{\Delta T^{\text{hyst}}}{2} (t - t_i) & \text{for } t_i \leq t \leq t_f; \\ \pm |q_{si}(t_f)| e^{-\frac{t-t_f}{\tau_c}} & \text{for } t > t_f \end{cases} \quad (18)$$

where the “+” sign holds in a heating process so that $q_{si}(t) > 0$, the “-” sign holds for the cooling case so that $q_{si}(t) < 0$, $|q_{si}(t_f)| = \lambda^3 c_s \Delta T^{\text{hyst}} (t_f - t_i) / (2\tau_c \tau_{si})$ is the heat flux at the end of the phase transition when $t = t_f$ and $\Delta T^{\text{hyst}} = T_{hi} - T_{ci} > 0$ is the temperature hysteresis between the heating, i.e. T_{hi} , and cooling, i.e. T_{ci} ,

transition temperatures of each avalanche. In particular, for the sake of simplicity, in what follows we will assume ΔT^{hyst} to be the same for all the avalanches detected at a given field H , meaning that the temperature hysteresis depends only on H but not on the single microscopic irreversible events i driving the transition, and moreover we will choose T_{hi} and T_{ci} to be symmetric around T_t (see Fig. 2). This way $T_t = (T_{hi} + T_{ci})/2$ and $\Delta T^{\text{hyst}}/2 = T_{hi} - T_t = T_t - T_{ci}$.

It is important to point out that in the case of slow scan rates and far-from-equilibrium avalanches that we are considering, the theoretically expected behaviour of the heat flux signal during the transition, i.e. for $t_i \leq t \leq t_f$, is linear in time and governed by both the time constants τ_{si} and τ_c , while the subsequent relaxation towards the equilibrium is described by an exponential law governed by the time constant τ_c alone, related to the thermal contact details only.

IV. COMPARISON WITH EXPERIMENTS

We have analyzed the experimental data obtained by performing Peltier calorimetry temperature scans at different rates and at various applied magnetic fields H on a series of $\text{La}(\text{Fe-Mn-Si})_{13}\text{-H}_{1.65}$ samples. Indeed, this kind of experiments, in which a calorimeter evaluates the heat flux exchanged between the sample and the external thermostat by performing temperature or magnetic field scans at different rates^{61,62}, are the right ones to apply the theoretical model developed in Sec. III. The sample preparation and the experimental procedure followed to detect the heat flux signals are detailed in Ref. [55]. In particular, in Ref. [55] it has been shown that the heat flux signals present well separated avalanches only when the temperature scans are performed at very low rates, i.e. lower than 20 mK/s, on small fragments of the material under investigation characterized by a mass of few milligrams. We have focused our analysis on the data obtained through scans performed in heating at the lowest scan rate, i.e. $dT_b/dt = 1$ mK/s, on two samples of the series characterized by nominal compositions Mn=0.18 and Mn=0.30. The mass of the samples is $m_1 = 4.79$ mg and $m_2 = 5.26$ mg for the two compositions 0.18 and 0.30, respectively. It is worth noting that such small masses allows us to assume from here on that $\lambda = L$, meaning that the sample temperature T will be considered as uniform within the whole sample.

The resulting heat flux signals as a function of time for different fields H varying between 0 T and 1.5 T and around the transition temperature T_t are reported in Fig. 4. The data clearly show the presence of avalanches separated in time in both the samples, increasing in number and changing in shape by approaching the critical field H_c of the system, at which the phase transition becomes second order, given by $H_c \simeq 2.3$ T and $H_c \simeq 1.2$ T for Mn=0.18 and Mn=0.30, respectively⁶³. All the avalanches are characterized by a fast linear growth fol-

lowed by a longer exponential decay. To interpret theoretically this kind of behaviour we can notice that since the experimental temperature scans are performed at a very low rate for each field H , we can safely treat the thermostat temperature T_b as constant during the phase transition. Then, we have described the time behaviour of the avalanches by Eq. (18) of Sec. III B.

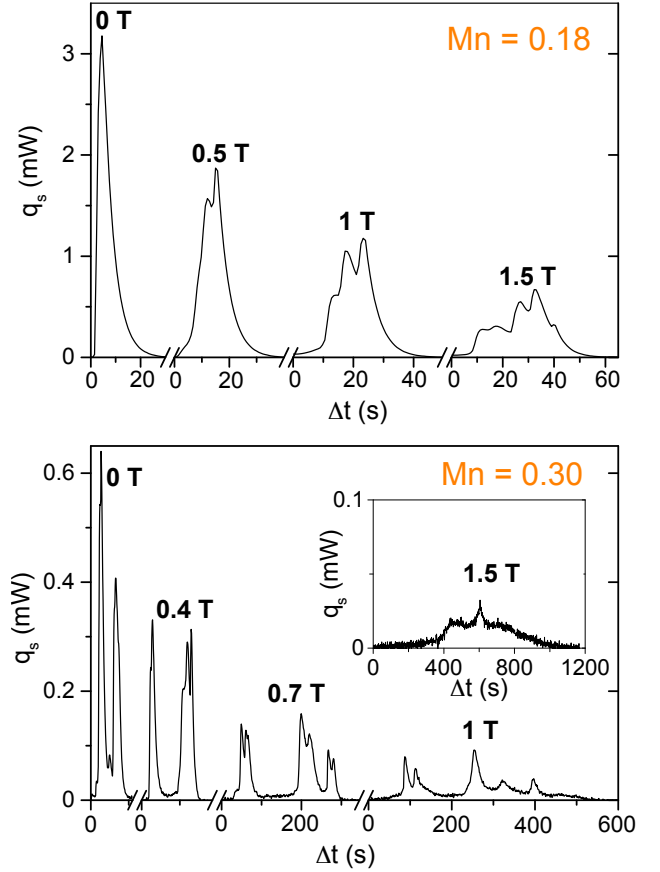


Fig. 4. Heat flux q_s as a function of time at different magnetic fields $\mu_0 H$. Experimental data obtained by Peltier calorimetry temperature scans performed at $dT_b/dt = 1$ mK/s rate, upon heating, on $\text{LaFe}_{11.60}\text{Mn}_{0.18}\text{Si}_{1.22}\text{-H}_{1.65}$ (top) and $\text{LaFe}_{11.41}\text{Mn}_{0.30}\text{Si}_{1.29}\text{-H}_{1.65}$ (bottom) samples.

We have first of all obtained the values of τ_c by performing the fit of the exponential decays observed in selected avalanches of both samples at various H , as shown in Fig. 5. The resulting average values $\langle \tau_c \rangle$ for the various H and Mn compositions are reported in Table I. We have then fitted the linear rises with the function $q_{si}(t) = a(t - t_i)$. From the first equation in Eq. (18), the slope a can be written as $a = (R_{si}/\tau_c) \Delta T^{\text{hyst}}/2$, where we have defined the quantity $R_{si} = (\alpha_s A_i)^{-1} = (\alpha_s \ell_i^2)^{-1}$, having the units of a thermal resistance, i.e. K/W. In particular, from the definition of R_{si} we can notice that it accounts only for the internal damping mechanism driving the system through the phase transition, but not for the contact details. The choice of evaluating R_{si} instead of τ_{si} lies on the difficulty to estimate the reversible con-

tribution to the specific heat of the system c_s close to the transition temperature T_t . By using the values of τ_c and those of the temperature hysteresis $\Delta T^{\text{hyst}}/2$ experimentally determined^{55,63} and reported in Table I and Fig. 7, it is possible to evaluate R_{si} . The behaviour of R_{si} for the avalanches analyzed is reported in Fig. 6, panel (a).

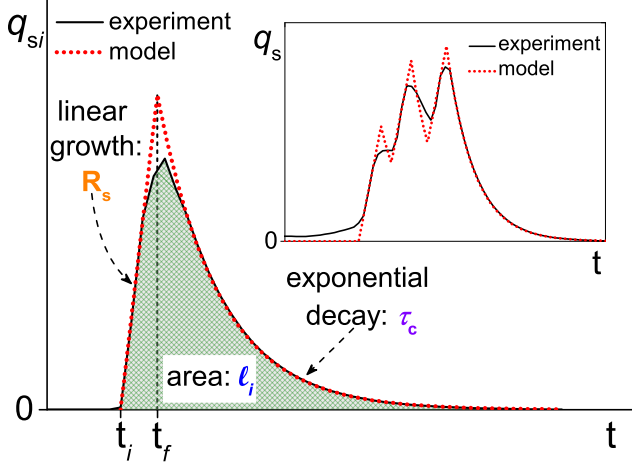


Fig. 5. Example of the fit of an individual avalanche: fitting curve according to Eq. (18) (red dotted line) and experimental data (black solid line). The fit of linear rise, exponential decay, and area under the curve, allow to determine the parameters R_{si} , τ_c and ℓ_i , respectively. *Inset*: example of the fit in the case of a multiple avalanche.

In order to evaluate the damping coefficient α_s we need to evaluate the linear size ℓ_i associated to each resistance value R_{si} . ℓ_i has been obtained by computing the latent heat exchanged by each region of the sample involved in the phase transition with the surroundings. As shown in Sec. II B, the latent heat is related to the volume $\ell_i A_i \sim \ell_i^3$ covered by the boundary interface during its motion through Eq. (8), so that $\ell_i = [(\int q_{si}(t) dt) / \Delta u_L]^{1/3}$. Thus, by integrating the individual heat flux avalanches detected experimentally (see Fig. 4) between the times corresponding to the beginning of the avalanche and to the end of its exponential decay (see Fig. 5), and by using the experimental values for $\Delta u_L = T_t \Delta s_L$ reported in Table I (see also Fig. 7), we have found ℓ_i values reported in the panel (b) of Fig. 6.

Finally, we have evaluated the damping coefficient α_s through the internal resistance R_{si} and the size ℓ_i as $\alpha_s = 1/(R_{si} \ell_i^2)$. This way we can estimate also the starting velocity of the boundary interface $v = dx/dt = (\alpha_s / \Delta u_L) \Delta T^{\text{hyst}}/2$, a relation obtained by approximating Eq. (9) for $T \simeq T_t$. The behaviour of v , together with the values of the ratio $\alpha_s / \Delta u_L$, are shown in the panels (c) and (d) of Fig. 6 at various magnetic fields H and different Mn compositions.

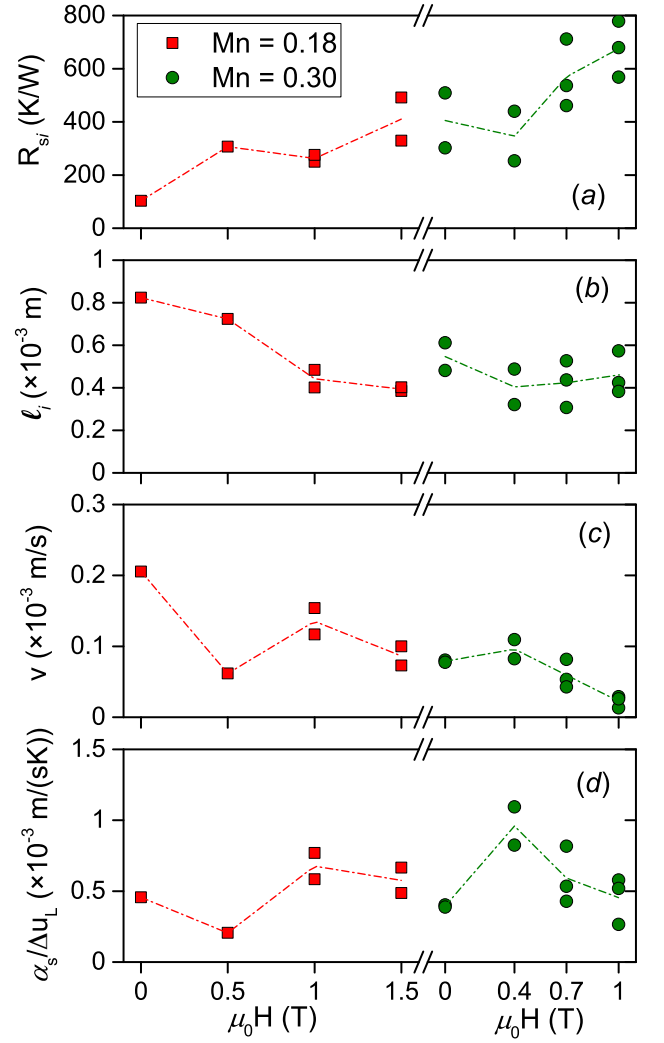


Fig. 6. Damping resistance R_{si} (a), linear size ℓ_i (b), velocity $v = dx/dt$ (c) and ratio $\alpha_s / \Delta u_L$ (d), as a function of the applied field $\mu_0 H$, for $\text{La}(\text{Fe-Mn-Si})_{13}\text{-H}$ samples with nominal compositions $\text{Mn}=0.18$ (red squares) and $\text{Mn}=0.30$ (green circles). Points obtained by fitting the avalanches shown in Fig. 4 through Eq. (18) with the parameters reported in Table I. Dash-dotted lines connecting the average values among points are guides to the eyes.

V. DISCUSSION

As a first result of the fitting of the experimental avalanches with the model, we can observe that R_{si} , beyond depending on the Mn composition, increases by increasing the applied magnetic field H (panel (a) in Fig. 6). The opposite behaviour characterizes the typical size ℓ_i swept out by each piece of the domain boundary interface during its motion (panel (b) in Fig. 6). Such a decrease in ℓ_i , and hence in the volume ℓ_i^3 of each individual avalanche, is consistent with the increase in the number of avalanches which are experimentally detected when approaching the critical point of the system (see

Mn=0.18					Mn=0.30				
$\mu_0 H$ [T]	T_t [K]	$\Delta T^{\text{hyst}}/2$ [K]	Δu_L [$\times 10^6 \text{ J/m}^3$]	$\langle \tau_c \rangle$ [s]	$\mu_0 H$ [T]	T_t [K]	$\Delta T^{\text{hyst}}/2$ [K]	Δu_L [$\times 10^6 \text{ J/m}^3$]	$\langle \tau_c \rangle$ [s]
0	321.4	0.45	31.2	4.0	0	295.8	0.2	21.9	6.1
0.5	323.1	0.3	30.2	4.1	0.4	297.6	0.1	20.1	5.8
1	325.1	0.2	29.3	4.2	0.7	298.6	0.1	18.3	10.5
1.5	326.7	0.15	28.2	4.6	1	300.5	0.05	16.9	22.0

Table I. Experimental values of T_t , $\Delta T^{\text{hyst}}/2$ and $\Delta u_L = T_t \Delta s_L$, obtained by Peltier calorimetry temperature scans at different magnetic fields $\mu_0 H$ on La(Fe-Mn-Si)₁₃-H samples with Mn=0.18 and Mn=0.30 (density $\rho = 7200 \text{ kg/m}^3$), after Refs. [55,63]. The average values $\langle \tau_c \rangle$ are evaluated by fitting the decay parts of the heat flux avalanches (Fig. 4) with the exponential law of Eq. (18), as depicted in Fig. 5.

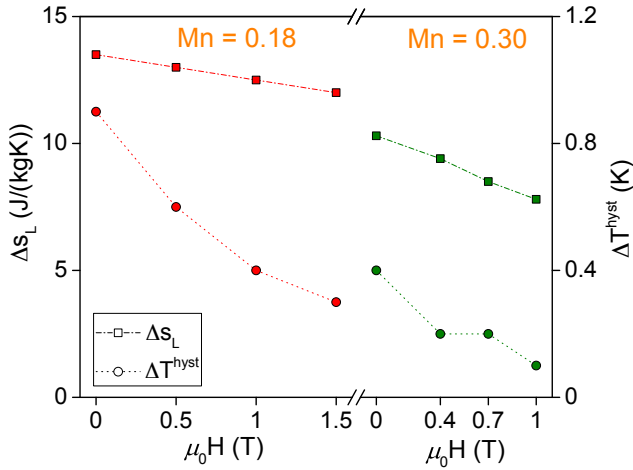


Fig. 7. Experimental values of entropy change per unit mass Δs_L at T_t (squares; scale on left axis) and of temperature hysteresis ΔT^{hyst} (circles; scale on right axis), as a function of the applied field $\mu_0 H$, for La(Fe-Mn-Si)₁₃-H compounds with nominal compositions Mn=0.18 (red) and Mn=0.30 (green).

Fig. 4), since the volume that transforms during the transition from a certain phase to a new one is $\lambda^3 \sim \sum_i \ell_i^3$.

This kind of behaviour is not trivial and it may be interpreted as the consequence of the assumption that the transition is driven by the heterogeneous nucleation and pinning of the boundaries of the new phase at the defects present in the MCE sample. The applied field H can be thought of as acting on the typical energy profile characterizing a first order transition (Fig. 2) by modulating the energy barrier between the stable phases S_0 and S_1 and hence by decreasing the temperature hysteresis ΔT^{hyst} , as shown in the bottom of Fig. 7, without affecting the material microstructure. This way it is possible to distinguish three different regimes according to the values of the applied field H . When H is far below the critical point and eventually $H \sim 0$, the energy barrier and the hysteresis are high enough to prevent many defects of the sample to be active as nucleation centres of the new phase. As a consequence, when the new phase nucleates at a certain point, the subsequent transformation

involves the whole sample and a single avalanche is observed. At higher H but still below H_c , the energy barrier and ΔT^{hyst} are reduced and the nucleation and growth of new domains may occur in several points of the sample. Then, more avalanches, still well separated in time, come into play and are experimentally detected. Finally, by further increasing H and getting closer to H_c or even above it, the hysteresis reduces essentially to zero and a proliferation of avalanches superimposing each other is observed. The number of avalanches is so high that they are blurred in an almost continuous background and the single peaks cannot be distinguished anymore.

The situation here described can be efficiently enlightened by choosing several samples having different critical points H_c , so that a given applied field H may be either well below H_c , or at an intermediate level between 0 and H_c , or finally close or higher than H_c , according to the specific sample under investigation. This situation is well represented by the compounds of the La(Fe-Mn-Si)₁₃-H_{1.65} series that we have considered here. Indeed, an applied field $H \sim 1.5 \text{ T}$ is already higher than $H_c \sim 1.2 \text{ T}$ for the Mn=0.30 sample, but it is still below $H_c \sim 2.3 \text{ T}$ in the case Mn=0.18. This circumstance is well reflected in the behaviour of the heat flux signals detected at this field on the two compounds. These signals show indeed a pattern already structured in separated avalanches for Mn=0.18 and, on the contrary, a rather continuous background for Mn=0.30 (Fig. 4 and inset therein).

Interestingly, the increase in R_{si} and the decrease in ℓ_i observed by increasing H compensate each other, so that the parameter $\alpha_s/\Delta u_L = (R_{si}\ell_i^2\Delta u_L)^{-1}$ appearing in Eq. (9) is essentially constant, independently on H and on the material composition (Fig. 6, panel (d)). The average value of this parameter, representing the starting velocity of the moving phase boundary interface corresponding to a variation in temperature of 1 K, amounts to $\alpha_s/\Delta u_L \approx 0.5 \times 10^{-3} \text{ (m/s)/K}$.

Another important feature to mention is that the velocity $v = dx/dt$ of the heat flux avalanches shows a clear decrease by enhancing H and getting closer to H_c (panel (c) in Fig. 6), meaning that the associated bound-

ary motion slows down by approaching the critical point of the system. This kind of behaviour may be interpreted as a manifestation of the critical slowing down known to appear around the critical point of a phase transition^{64,65} and it can be ascribed to the disappearance of the avalanches above H_c .

A final comment concerns the role played by the intrinsic kinetics governing the transition, with respect to extrinsic factors, in affecting the heat exchanged between the MCE sample and the surroundings. A comparison between the R_{si} values and the contact resistance values R_c can be made. A rough estimate of R_c can be obtained from the average values $\langle\tau_c\rangle$ reported in Table I for different fields H and nominal Mn compositions. In order to relate R_c to $\langle\tau_c\rangle$ we must take into account the fact that for the particular measuring setup we have employed to perform the temperature scans, the thermal contacts comprise also the Peltier cells of the calorimeter which are characterized by their own resistance and capacity R_P and C_P , respectively. Both these quantities can be determined by calibrating the calorimeter and they evaluate to $R_P = 75 \text{ K/W}$ and $C_P = 48 \text{ mJ/K}$ ⁶². Then, by including also the contribution associated to C_P , the thermal contact resistance can be expressed as $R_c = \langle\tau_c\rangle / (C_s + C_P)$. The heat capacity $C_s = \lambda^3 c_s$ may be evaluated by observing that λ^3 represents in our case the whole sample volume, since we have assumed $\lambda = L$, and the specific heat c_s around the transition temperature at various H can be extrapolated from the experimental data reported in Ref. [63]. With $c_s \simeq 600 \text{ J/(kg K)}$ for Mn=0.18, essentially independent on H , and $c_s \simeq 1000 \text{ J/(kg K)}$ at $H = 0 \text{ T}$ and $c_s \simeq 1500 \text{ J/(kg K)}$ at $H = 1 \text{ T}$ for Mn=0.30, we can conclude that $R_c \sim 80\text{--}90 \text{ K/W}$ in the Mn=0.18 case, while $R_c \sim 100\text{--}400 \text{ K/W}$ for Mn=0.30. We can notice that the R_c and R_{si} values have the same order of magnitude for both the compositions here considered. We can conclude that it would be attractive to envisage the development of experiments able to enhance R_c with respect to R_{si} , or viceversa, by choosing the right MCE materials and measuring setup. This way it would be possible to clearly distinguish the effects, on the heat flux exchange, due to the intrinsic kinetics and to the extrinsic factors, as the measurement system. Such an investigation will be the matter of future works.

VI. CONCLUSIONS

In the present paper we have introduced a thermodynamic model describing the out-of-equilibrium effects proper of first order phase transitions to analyze the heat flux signals experimentally observed by performing temperature scans at low rate on a series of $\text{La(Fe-Mn-Si)}_{13}\text{-H}_{1.65}$ fragments with Mn=0.18 and Mn=0.30. The physical picture arising from the comparison between the experimental data and the model is coherent with the assumption of a defects-driven phase transition, in which the system transforms from a magnetically ordered LT-

FM phase to a disordered HT-PM phase because of the motion of the domain boundaries which nucleate at the defects present in the material microstructure.

In particular, we have shown that when the scan rate is low enough, the nucleation and pinning centres of the sample are active one at a time and they give rise to characteristic repeatable series of heat flux peaks which have a typical linear growth followed by an exponential decay. We have related the appearance of these avalanches to individual, well time-separated, independent boundary motion events associated to the latent heat of the system. Furthermore, we have shown that the non trivial patterns experimentally observed in the heat flux signals can be interpreted as a consequence of the applied magnetic field H . The latter modulates the energy profile and the hysteresis of the system by getting closer to the critical point H_c and it affects this way the number of nucleation centres that may be active into the sample.

Finally, we have evaluated the coefficient α_s associated to the internal damping of the boundary motion events for the $\text{La(Fe-Mn-Si)}_{13}\text{-H}_{1.65}$ compounds. Although a precise quantitative estimate of this parameter is limited by the low number of available experimental data, we have found a value α_s which is essentially independent on both the applied magnetic field H and the Mn composition. This outcome suggests that α_s may be considered as a parameter related only to the intrinsic properties of each class of MCE materials.

Appendix A: Constant T_b

The case of a constant thermal reservoir temperature T_b allows to properly describe calorimetry measurements in which the temperature scans are performed at very low rates. In this regime the single avalanches observed in the heat flux signal are well separated in time and distinguishable from a uniform background, so that it is possible to follow the time evolution of each of them. The appearance of each avalanche is due to individual nucleation and pinning events occurring in many different regions of the sample which are active at different subsequent times. The separation in time of these events can be explained by supposing that when the transition begins, the phase boundary interface will start to move around a certain nucleation centre, exchanging heat and causing the variation of the sample temperature T within a typical volume λ^3 (see Fig. 3) around the nucleation centre. This change in temperature will prevent the occurrence of other nucleation events and boundary motions inside the same volume, since T will be different from the threshold value necessary for the motion of the boundary interface, i.e. T_{hi} in an heating process or T_{ci} in the cooling case (see Sec. II B). Once the phase boundary will stop and the heat flux avalanche will end, the whole region will relax again towards the equilibrium temperature T_{hi} or T_{ci} , thus allowing a new avalanche to start. The presence of an applied magnetic field H does

not affect this picture, even if H is close to the critical value H_c . Indeed, the increase in the H value is reflected into a decrease of the temperature hysteresis ΔT^{hyst} and in the consequent increase of the number of the active regions of the sample in which an avalanche event may occur. Therefore, by increasing H the number of individual avalanches experimentally detected is also increased. However, the separation in time among these avalanches depends on the heat exchanged by the boundary interface with the surrounding region of the sample and with the external thermal reservoir and this feature is related only to the internal properties of the material and to the external scan rate, but it cannot be affected by H .

The differential equations governing the time behaviour of the sample temperature $T(t)$ have been derived in Sec. III and are given by Eqs. (16)–(17). To solve these equations we assume that the transition starts at $T(t_i) = T_{hi}$ for an heating process ($T(t_i) = T_{ci}$ for the cooling case). Then the constant T_b value is $T_b = T_{hi}$ in heating ($T_b = T_{ci}$ in cooling). The solution of Eqs. (16)–(17) for an individual avalanche is then

$$T(t) = \begin{cases} T(t_i) \mp \frac{\tau_c}{\tau_c + \tau_{si}} \frac{\Delta T^{\text{hyst}}}{2} \left(1 - e^{-\frac{t-t_i}{\tau_{sc}}}\right) & \text{for } t_i \leq t \leq t_f; \\ T(t_i) \mp |T(t_i) - T(t_f)| e^{-\frac{t-t_f}{\tau_c}} & \text{for } t > t_f, \end{cases} \quad (\text{A1})$$

where $T(t_i) = T_{hi}$ and the “-” sign hold for an heating process, while $T(t_i) = T_{ci}$ and the “+” sign hold in the cooling case and we have introduced the quantity $|T(t_i) - T(t_f)| = \tau_c / (\tau_c + \tau_{si}) (\Delta T^{\text{hyst}} / 2) [1 - e^{-(t_f-t_i)/\tau_{sc}}] > 0$, with $\Delta T^{\text{hyst}} = T_{hi} - T_{ci}$ and $\Delta T^{\text{hyst}} / 2 = T_{hi} - T_t = T_t - T_{ci}$. Moreover, in Eq. (A1) we have defined the time constant $\tau_{sc} = (1/\tau_c + 1/\tau_{si})^{-1} = \lambda^3 c_s (\lambda^2 \kappa_c / t_c + \alpha_s \ell_i^2)^{-1}$. We observe that the time constant τ_{sc} , governing the behaviour of T during the transition, is the parallel of the time constants τ_c, τ_{si} defined in Sec. III B and therefore it is dominated by the smaller one between them. This observation implies that the heat exchanged between the boundary interface and the surrounding region of the sample during the phase transition can be governed either by the intrinsic damping ($\tau_{si} \ll \tau_c$) or by external factors only ($\tau_{si} \gg \tau_c$). In particular, since we are assuming that $\ell_i \ll \lambda$ (see Sec. III B and Fig. 3) and that the contact resistance $t_c / (\kappa_c A_c)$ for the samples here investigated is low (see Ref. [55]), the internal time constant τ_{si} shall be expected to be higher than the τ_c for any event i , so that $\tau_{sc} \simeq \tau_c$. In this respect, it is worth noting that from an analytical point of view the time constants τ_{si} and τ_c can be independently determined and do not mix together if the individual heat flux avalanches associated to the transition event are far from equilibrium during the whole transition, a condition which is realized if $t_f - t_i \ll \tau_{sc}$. Indeed, in this case we have that $\exp[-(t - t_i)/\tau_{sc}] \simeq 1 + (t - t_i)/\tau_{sc}$ and the first row of Eq. (A1) assumes the form $T(t) - T(t_i) \simeq \mp (\Delta T^{\text{hyst}} / 2) (t - t_i) / \tau_{si}$ independently on whether $\tau_{si} \ll \tau_c$ or $\tau_{si} \gg \tau_c$. Then,

we can conclude that in the case of far-from-equilibrium avalanches, the sample temperature T will vary linearly in time with a slope determined only by the internal time constant τ_{si} for $t_i \leq t \leq t_f$, while it will relax back to the equilibrium for $t > t_f$ with an exponential law governed only by the time constant τ_c .

The solution given by Eq. (A1), combined with Eq. (14), allows to determine the time behaviour of the heat current density $j_q(t)$ flowing through the thermal contact for an individual avalanche event, which reads:

$$j_q(t) = \begin{cases} \mp \frac{\lambda c_s}{\tau_c + \tau_{si}} \frac{\Delta T^{\text{hyst}}}{2} \left(1 - e^{-\frac{t-t_i}{\tau_{sc}}}\right) & \text{for } t_i \leq t \leq t_f; \\ \mp |j_q(t_f)| e^{-\frac{t-t_f}{\tau_c}} & \text{for } t > t_f, \end{cases} \quad (\text{A2})$$

with $|j_q(t_f)| = \lambda c_s |T(t_i) - T(t_f)| / \tau_c$ being the modulus of the heat current density at $t = t_f$, the “-” sign holding for an heating process and the “+” sign holding for the cooling case.

Finally, from Eq. (A2) and by integrating the continuity equation Eq. (13) on the volume λ^3 enclosed in a surface area λ^2 , we obtain the time behaviour of an individual heat flux avalanche $q_{si}(t) = -\lambda^2 j_q(t)$:

$$q_{si}(t) = \begin{cases} \pm \frac{\lambda^3 c_s}{\tau_c + \tau_{si}} \frac{\Delta T^{\text{hyst}}}{2} \left(1 - e^{-\frac{t-t_i}{\tau_{sc}}}\right) & \text{for } t_i \leq t \leq t_f; \\ \pm |q_{si}(t_f)| e^{-\frac{t-t_f}{\tau_c}} & \text{for } t > t_f, \end{cases} \quad (\text{A3})$$

where, in this case, $|q_{si}(t_f)| = \lambda^3 c_s |T(t_i) - T(t_f)| / \tau_c$ is the modulus of the the heat flux at $t = t_f$, the “+” sign holds in heating so that $q_{si}(t) > 0$ and the “-” sign holds in cooling so that $q_{si}(t) < 0$. Again, if the avalanches are far from equilibrium and hence $t_f - t_i \ll \tau_{sc}$, the heat flux behaviour during the transition becomes linear in time and governed by both the time constants τ_{si} and τ_c , while the subsequent relaxation towards equilibrium will still be described by an exponential law governed by the time constant τ_c related to the thermal contact details only:

$$q_{si}(t) = \begin{cases} \pm \frac{\lambda^3 c_s}{\tau_c \tau_{si}} \frac{\Delta T^{\text{hyst}}}{2} (t - t_i) & \text{for } t_i \leq t \leq t_f; \\ \pm |q_{si}(t_f)| e^{-\frac{t-t_f}{\tau_c}} & \text{for } t > t_f \end{cases} \quad (\text{A4})$$

with $|q_{si}(t_f)| = \lambda^3 c_s \Delta T^{\text{hyst}} (t_f - t_i) / (2\tau_c \tau_{si})$.

Appendix B: T_b varying at constant rate \dot{T}_b

The case of a thermal reservoir temperature T_b varying at a constant rate \dot{T}_b applies to the description of calorimetry experiments performed at high scan rates. Contrary to the case discussed in Appendix A, the high scan rate allows many regions surrounding different domain nucleation centres inside the MCE sample to be

active at the same time and not independent one of each other. As for Appendix A, each of these regions will contribute to develop the phase boundary interface with a portion of surface having area A_i and it will affect the sample temperature T within a volume λ^3 around the nucleation centre. However, the main difference with respect to the case of a thermal reservoir kept at a constant temperature T_b treated in Appendix A is represented by the fact that many irreversible events i , each one associated to the motion of a single piece of surface A_i , will occur concurrently within the volume λ^3 . This happens because the heat provided by the reservoir at high scan rates is high enough to balance the change in temperature occurring in the λ^3 volume because of the phase boundary motion, so that the threshold temperatures T_{ci} , T_{hi} (see Sec. IIB) will be overcome almost simultaneously by many nucleation centres. Then, all the terms proportional to A_i appearing in the sum on the right-hand side of Eq. (15) must be taken into account and, since the damping coefficient α_s , the typical size λ and the transition temperature T_t are the same for all the events, we can write the area of the phase boundary interface as $A = \sum_i A_i = \sum_i \ell_i^2$ (see also Sec. IIC). The time constant related to the damping mechanism associated to the motion of the whole surface A is in this case denoted as τ_s and it reads $\tau_s = \lambda^3 c_s / (\alpha_s \sum_i \ell_i^2) = \sum_i \tau_{si}$, where τ_{si} is the time constant, defined in Sec. IIIB, which refers to the damping of a portion A_i only of the whole boundary interface. It is worth noting that depending on the upper limit in the previous sum, it can be either $A_i \sim A$ if the limit is low or $A_i \ll A$ if the limit is high enough. In the former case we can assume $\tau_s \sim \tau_{si} = \lambda^3 c_s / (\alpha_s \ell_i^2)$, while in the latter case we have $\tau_s \ll \tau_{si}$. More important, although $A_i \ll \lambda^2$ since we are assuming $\ell_i \ll \lambda$, it may happen that A , being the sum of many A_i , will be greater than λ^2 , so that also $\tau_c > \tau_s$. Hence, with respect to the constant T_b case, in the fast scan rate regime there is also the possibility that the heat exchanged between the MCE sample and the external thermal reservoir may be primarily governed by the thermal contact details instead of the intrinsic kinetics of the phase transition.

From the experimental point of view, the heat flux signal $q_s(t)$ detected in this regime is not characterized anymore by individual peaks well separated in time associated to the different events i as it was for the case of a constant T_b , but it rather shows a continuous behaviour due to the superposition of many concurrent events. It is worth noting that in this case also the times t_i , t_f at which the phase transition begins and ends, respectively, identify the length in time of the whole heat flux signal composed by many superimposed avalanches and not only the time span of an individual single avalanche, as it was in Sec. IIIB and in Appendix A. Moreover, the shape of q_s is also highly affected by the magnetic field H which plays here a prominent role, since it determines the number of irreversible events i occurring in the sample at the same time. Indeed, as discussed in Appendix A, while H is approaching the critical value H_c , the temperature hysteresis ΔT^{hyst} reduces and thus the number of active regions in which new domains nucleate and growth is increased. This means that also the number of terms contributing to the sum appearing in Eq. (15) is increased and this fact is reflected on the behaviour of the sample temperature $T(t)$ and of the heat flux signal $q_s(t)$.

To solve Eqs. (16)–(17) in the case of a thermal bath temperature varying in time as $T_b(t) = T_b(t_i) + \dot{T}_b(t - t_i)$ for $t > t_i$, with $\dot{T}_b > 0$ in an heating process or $\dot{T}_b < 0$ in a cooling case, we must determine first of all the initial value $T_b(t_i)$. To this aim, we observe that before the transition starts, i.e. for $t \leq t_i$, the sample temperature T has a small lag behind T_b due to the contact resistance $t_c/(\kappa_c A_c)$ between the MCE sample and the reservoir. Then, we can conclude that $T_b(t) = T(t) + \tau_c \dot{T}_b$ for $t \leq t_i$. At $t = t_i$, the sample temperature reaches the threshold value $T(t_i) = T_h$ in an heating process or $T(t_i) = T_c$ in the cooling case, so that the initial condition on T_b reads $T_b(t_i) = T_h + \tau_c \dot{T}_b$ in heating and $T_b(t_i) = T_c + \tau_c \dot{T}_b = T_c - \tau_c |\dot{T}_b|$ in cooling.

With the above conditions and the time constant τ_{sc} defined as in Eqs. (A1)–(A2)–(A3) but with τ_{si} replaced in this case by τ_s , the solution $T(t)$ of Eqs. (16)–(17) and the heat flux $q_s(t)$ read

$$T(t) = \begin{cases} T(t_i) + \frac{\tau_s}{\tau_c + \tau_s} \dot{T}_b(t - t_i) \mp \frac{\tau_c}{\tau_c + \tau_s} \left(\frac{\Delta T^{\text{hyst}}}{2} - \tau_{sc} |\dot{T}_b| \right) \left(1 - e^{-\frac{t-t_i}{\tau_{sc}}} \right) & \text{for } t_i \leq t \leq t_f; \\ T(t_i) - (T(t_i) - T(t_f)) e^{-\frac{t-t_f}{\tau_c}} + \dot{T}_b(t_f - t_i) \left(1 - e^{-\frac{t-t_f}{\tau_c}} \right) + \dot{T}_b(t - t_f) & \text{for } t > t_f; \end{cases} \quad (\text{B1})$$

$$q_s(t) = \begin{cases} \pm \frac{\lambda^3 c_s}{\tau_c} \left[\tau_c |\dot{T}_b| + \frac{\tau_c}{\tau_c + \tau_s} |\dot{T}_b| (t - t_i) + \frac{\tau_c}{\tau_c + \tau_s} \left(\frac{\Delta T^{\text{hyst}}}{2} - \tau_{sc} |\dot{T}_b| \right) \left(1 - e^{-\frac{t-t_i}{\tau_{sc}}} \right) \right] & \text{for } t_i \leq t \leq t_f; \\ q_s(t_f) e^{-\frac{t-t_f}{\tau_c}} + \lambda^3 c_s \dot{T}_b \left(1 - e^{-\frac{t-t_f}{\tau_c}} \right) & \text{for } t > t_f. \end{cases} \quad (\text{B2})$$

where the “ $-$ ” sign in Eq. (B1) and the “ $+$ ” sign in

Eq. (B2) hold in heating, while the opposite signs in the

same equations hold for cooling. Moreover, in analogy with Appendix A, we have set $\Delta T^{\text{hyst}} = T_h - T_c$ and $\Delta T^{\text{hyst}}/2 = T_h - T_t = T_t - T_c$. In particular, we observe that Eq. (B2) is evaluated by combining Eq. (B1) with Eqs. (13)–(14), following the same procedure used in Appendix A to obtain Eq. (A3). The heat current density $j_q(t)$, analogous to Eq. (A2), is simply obtained from Eq. (B2) as $j_q(t) = -q_s(t)/\lambda^2$.

There are two special limits of Eqs. (B1)–(B2) that deserve attention and allow to simplify the above expressions, namely the case in which the sample temperature $T(t)$ and the heat flux signals q_s are far from their equilibrium values for the whole phase transition, a condition realized whenever $t_f - t_i \ll \tau_{\text{sc}}$, and, on the opposite, the case in which T and q_s can be close and even reach the thermodynamic equilibrium during the transformation, i.e. $t_f - t_i \gtrsim \tau_{\text{sc}}$.

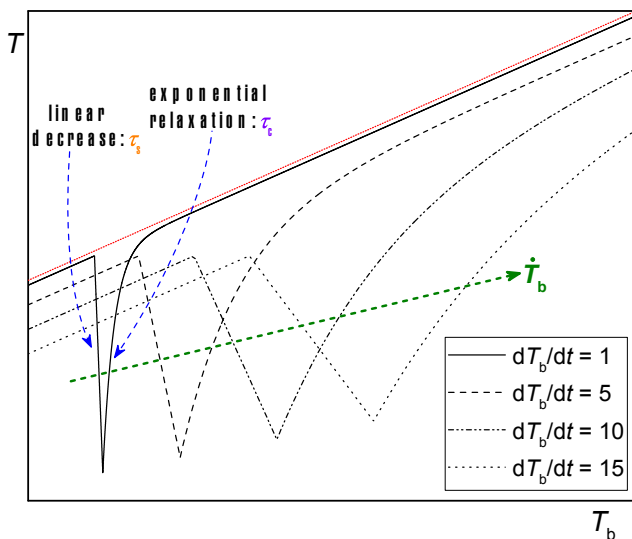


Fig. 8. Qualitative behaviour of T vs. T_b , for far-from-equilibrium signals at different rates $\dot{T}_b = dT_b/dt > 0$, according to Eq. (B3) for the linear decrease and Eq. (B1) (second row) for the exponential relaxation. The dotted red line shows the temperature T_b . \dot{T}_b values in the legend are expressed in arbitrary units.

a. Far-from-equilibrium signals. When the signals are far from the thermodynamic equilibrium, the behaviour of both $T(t)$ and $q_s(t)$ during the phase transition, i.e. for $t_i \leq t \leq t_f$, becomes linear in time, as it was for Eq. (A1) and Eq. (A3), and it is given by:

$$T(t) = T(t_i) + \dot{T}_b (t - t_i) \mp \frac{\Delta T^{\text{hyst}}}{2\tau_s} (t - t_i); \quad (\text{B3})$$

$$q_s(t) = \pm \lambda^3 c_s \left[|\dot{T}_b| + \frac{\Delta T^{\text{hyst}}}{2\tau_c \tau_s} (t - t_i) \right], \quad (\text{B4})$$

where in Eqs. (B3)–(B4) we have used the same convention on the signs as in Eqs. (B1)–(B2). Therefore, the far-from-equilibrium regime allows to clearly distinguish the role played by the time constants τ_s and τ_c in

determining the behaviour of $T(t)$ and $q_s(t)$ during and after the phase transition. Indeed, as shown in Eq. (B3), the slope in the linear behaviour of T during the phase transition is governed by the internal time constant τ_s only, independently on whether $\tau_c \ll \tau_s$ or, viceversa, $\tau_c \gg \tau_s$. For what concerns $q_s(t)$, Eq. (B4) shows furthermore that its linear behaviour is characterized by a slope determined by both the time constants τ_s and τ_c . When the transition is ended, i.e. for $t > t_f$, both T and q_s relax back to the thermodynamic equilibrium with an exponential law governed by τ_c only and described by Eqs. (B1)–(B2). The major difference with respect to the case of a constant T_b treated in Appendix A is that the behaviour of both $T(t)$ and $q_s(t)$ depends now also on the constant rate \dot{T}_b . This fact is qualitatively depicted in Fig. 8 and Fig. 9 where the sample temperature T and the heat flux q_s are reported, upon heating, as a function of the thermal bath temperature T_b at different rates $\dot{T}_b > 0$.

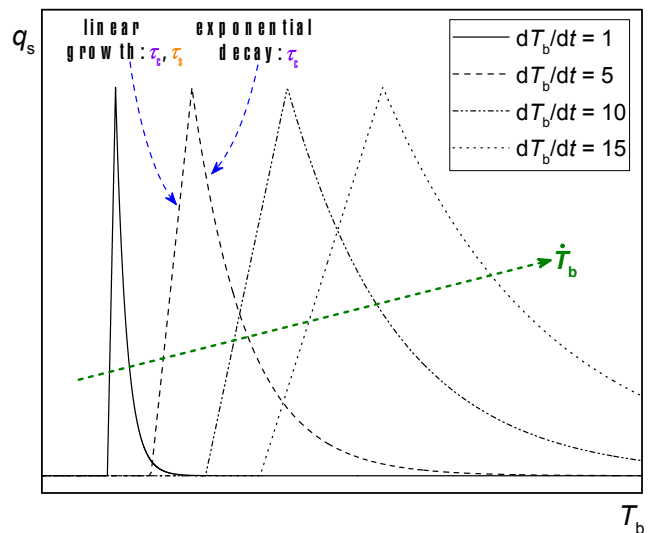


Fig. 9. Qualitative behaviour of q_s vs. T_b , for far-from-equilibrium signals at different rates $\dot{T}_b = dT_b/dt > 0$, according to Eq. (B4) for the linear growth and Eq. (B2) (second row) for the exponential decay. A constant offset $\lambda^3 c_s \dot{T}_b$ has been subtracted from all the curves. For the values in the legend see Fig. 8.

b. Close-to-equilibrium signals. The case of signals that can be close or even reach the thermodynamic equilibrium arises interestingly when the applied magnetic field H approaches the critical point H_c . Indeed, for $H \simeq H_c$ we have already noticed that $\tau_c > \tau_s$, so that $\tau_{\text{sc}} \simeq \tau_s$, being τ_{sc} the parallel between τ_c and τ_s . Since in this case we have also pointed out that $\tau_s \ll \tau_{s_i}$ and we know from the experimental results reported in Sec. IV that $\tau_{s_i} = \lambda^3 c_s R_{s_i} = C_s R_{s_i}$ is of the order of 10–100 ms, we may suppose that the heat flux signals last in time more than τ_s , i.e. $t_f - t_i \gtrsim \tau_{\text{sc}} \simeq \tau_s$. The linear approximation derived for the far-from-equilibrium signals regime does not hold anymore, but we can also in this case sim-

plify Eqs. (B1)–(B2) noting that now τ_s is negligible with

respect to τ_c . Then we obtain:

$$T(t) = \begin{cases} T(t_i) \mp \frac{\Delta T^{\text{hyst}}}{2} \left(1 - e^{-\frac{t-t_i}{\tau_s}}\right) \pm \tau_s |\dot{T}_b| \left(1 - e^{-\frac{t-t_i}{\tau_s}} + \frac{t-t_i}{\tau_c}\right) & \text{for } t_i \leq t \leq t_f; \\ T(t_i) - (T(t_i) - T(t_f))e^{-\frac{t-t_f}{\tau_c}} + \dot{T}_b (t_f - t_i) \left(1 - e^{-\frac{t-t_f}{\tau_c}}\right) + \dot{T}_b (t - t_f) & \text{for } t > t_f; \end{cases} \quad (\text{B5})$$

$$q_s(t) = \begin{cases} \pm \lambda^3 c_s \left[|\dot{T}_b| + \frac{\Delta T^{\text{hyst}}}{2\tau_c} \left(1 - e^{-\frac{t-t_i}{\tau_s}}\right) + |\dot{T}_b| \frac{t-t_i}{\tau_c} - \frac{\tau_s}{\tau_c} |\dot{T}_b| \left(1 - e^{-\frac{t-t_i}{\tau_s}}\right) \right] & \text{for } t_i \leq t \leq t_f; \\ q_s(t_f)e^{-\frac{t-t_f}{\tau_c}} + \lambda^3 c_s \dot{T}_b \left(1 - e^{-\frac{t-t_f}{\tau_c}}\right) & \text{for } t > t_f. \end{cases} \quad (\text{B6})$$

We can notice from Eqs. (B5)–(B6) that $T(t)$ and $q_s(t)$ show in this regime an exponential behaviour both during and after the transition, governed by τ_s and τ_c separately. Even in this case, Eqs. (B5)–(B6) can be linearized as a function of the thermal reservoir temperature $T_b(t)$, if the time constant τ_s is small enough, so that we can consider $t - t_i \gg \tau_s$ and we can safely neglect the exponentials appearing in these equations for $t_i \leq t \leq t_f$. Then, the solutions describing the temperature and heat flux behaviour as a function of $T_b(t)$ during the phase

transition, i.e. for $t_i \leq t \leq t_f$, read:

$$T \simeq \frac{\tau_s}{\tau_c} T_b + T_t - \frac{\tau_s}{\tau_c} T(t_i) \simeq T_t; \quad (\text{B7})$$

$$q_s \simeq \frac{\lambda^3 c_s}{\tau_c} (T_b - T_t). \quad (\text{B8})$$

In particular, the most important feature encompassed in Eq. (B8) is represented by the fact that the heat flux q_s has a linear dependence on the thermal bath temperature T_b characterized by a slope which is independent on the rate \dot{T}_b .

A similar linear behaviour is obtained, but as a function of the time t , also at times well beyond the end of the transition, i.e. at $t \gg t_f$. In this case the time behaviour of T and q_s becomes again linear, as it was for $t \leq t_i$ before the transition started, and it is given by $T(t) = T_b(t) - \left[T(t_i) - T(t_f) + \dot{T}_b (t_f - t_i)\right] e^{-\frac{t-t_f}{\tau_c}} - \tau_c \dot{T}_b \simeq T_b(t) - \tau_c \dot{T}_b$ and $q_s(t) = \lambda^3 c_s [T_b(t) - T(t)] / \tau_c = \lambda^3 c_s \dot{T}_b$.

* Corresponding author. E-mail address: m.piazzi@inrim.it

¹ O. Gutfleisch, M. A. Willard, E. Brück, C. H. Chen, S. G. Sankar, and J. Ping Liu, “Magnetic Materials and Devices for the 21st Century: Stronger, Lighter, and More Energy Efficient,” *Adv. Mater.* **23**, 821 (2011).

² K. G. Sandeman, “Magnetocaloric materials: The search for new systems,” *Scr. Mater.* **67**, 566 (2012).

³ I. Takeuchi and K. Sandeman, “Solid-state cooling with caloric materials,” *Phys. Today* **68**, 48 (2015).

⁴ A. Kitanovski, J. Tušek, U. Tomc, U. Plaznik, M. Ozbolt, and A. Poredoš, *Magnetocaloric Energy Conversion: From Theory to Applications* (Springer International Publishing, Switzerland, 2015).

⁵ J. Lyubina, “Magnetocaloric materials for energy efficient cooling,” *J. Phys. D: Appl. Phys.* **50**, 053002 (2017).

⁶ P. Debye, “Einige Bemerkungen zur Magnetisierung bei tiefer Temperatur,” *Ann. Phys. (Berlin)* **81**, 1154 (1926).

⁷ W. F. Giauque, “A THERMODYNAMIC TREATMENT OF CERTAIN MAGNETIC EFFECTS. A PROPOSED METHOD OF PRODUCING TEMPERATURES CONSIDERABLY BELOW 1° ABSOLUTE,” *J. Am. Chem. Soc.* **49**, 1864 (1927).

⁸ K. A. Gschneidner Jr., V. K. Pecharsky, and A. O. Tsokol, “Recent developments in magnetocaloric materials,” *Rep. Prog. Phys.* **68**, 1479 (2005).

⁹ E. Brück, O. Tegus, D. T. Cam Thanh, N. T. Trung, and K. H. J. Buschow, “A review on Mn based materials for magnetic refrigeration: Structure and properties,” *Int. J. Refrig.-Rev. Int. Froid* **31**, 763 (2008).

¹⁰ B. G. Shen, J. R. Sun, F. X. Hu, H. W. Zhang, and Z. H. Cheng, “Recent Progress in Exploring Magnetocaloric Materials,” *Adv. Mater.* **21**, 4545 (2009).

¹¹ R. Caballero-Flores, V. Franco, A. Conde, K. E. Knipling, and M. A. Willard, “Optimization of the refrigerant capac-

- ity in multiphase magnetocaloric materials,” *Appl. Phys. Lett.* **98**, 102505 (2011).
- ¹² V. Franco, J. S. Blázquez, B. Ingale, and A. Conde, “The Magnetocaloric Effect and Magnetic Refrigeration Near Room Temperature: Materials and Models,” *Ann. Rev. Mater. Res.* **42**, 305 (2012).
 - ¹³ A. Smith, C. R. H. Bahl, R. Bjørk, K. Engelbrecht, K. K. Nielsen, and N. Pryds, “Materials Challenges for High Performance Magnetocaloric Refrigeration Devices,” *Adv. Energy Mater.* **2**, 1288 (2012).
 - ¹⁴ A. Smaïli and R. Chahine, “Thermodynamic investigations of optimum active magnetic regenerators,” *Cryogenics* **38**, 247 (1998).
 - ¹⁵ A. Sarlah, A. Kitanovski, A. Poredos, P. W. Egolf, O. Sari, F. Gendre, and Ch. Besson, “Static and rotating active magnetic regenerators with porous heat exchangers for magnetic cooling,” *Int. J. Refrig.-Rev. Int. Froid* **29**, 1332 (2006).
 - ¹⁶ J. B. Jensen, K. Engelbrecht, C. R. H. Bahl, N. Pryds, G. F. Nellis, S. A. Klein, and B. Elmegaard, “Modeling of parallel-plate regenerators with non-uniform plate distributions,” *Int. J. Heat Mass Transf.* **53**, 5065 (2010).
 - ¹⁷ J. B. Jensen, C. R. H. Bahl, K. Engelbrecht, B. Elmegaard, and N. Pryds, “Analysis of single blow effectiveness in non-uniform parallel plate regenerators,” *Int. J. Heat Mass Transf.* **54**, 4746 (2011).
 - ¹⁸ C. R. H. Bahl, K. Engelbrecht, R. Bjørk, D. Eriksen, A. Smith, K. K. Nielsen, and N. Pryds, “Design concepts for a continuously rotating active magnetic regenerator,” *Int. J. Refrig.-Rev. Int. Froid* **34**, 1792 (2011).
 - ¹⁹ K. Engelbrecht, K. K. Nielsen, and N. Pryds, “An experimental study of passive regenerator geometries,” *Int. J. Refrig.-Rev. Int. Froid* **34**, 1817 (2011).
 - ²⁰ L. Theil Kuhn, N. Pryds, C. R. H. Bahl, and A. Smith, “Magnetic refrigeration at room temperature - from magnetocaloric materials to a prototype,” *J. Phys.: Conf. Ser.* **303**, 012082 (2011).
 - ²¹ K. K. Nielsen, K. Engelbrecht, D. V. Christensen, J. B. Jensen, A. Smith, and C. R. H. Bahl, “Degradation of the performance of microchannel heat exchangers due to flow maldistribution,” *Appl. Therm. Eng.* **40**, 236 (2012).
 - ²² K. K. Nielsen, K. Engelbrecht, and C. R. H. Bahl, “The influence of flow maldistribution on the performance of inhomogeneous parallel plate heat exchangers,” *Int. J. Heat Mass Transf.* **60**, 432 (2013).
 - ²³ Z. Chen, Y. Utaka, and Y. Tasaki, “Measurement and numerical simulation on the heat transfer characteristics of reciprocating flow in microchannels for the application in magnetic refrigeration,” *Appl. Therm. Eng.* **65**, 150 (2014).
 - ²⁴ Y. Kotani, Y. Kansha, M. Ishizuka, and A. Tsutsumi, “Experimental investigation of an active magnetic regenerative heat circulator applied to self-heat recuperation technology,” *Appl. Therm. Eng.* **70**, 1202 (2014).
 - ²⁵ J. A. Lozano, K. Engelbrecht, C. R. H. Bahl, K. K. Nielsen, J. R. Barbosa Jr., A. T. Prata, and N. Pryds, “Experimental and numerical results of a high frequency rotating active magnetic refrigerator,” *Int. J. Refrig.-Rev. Int. Froid* **37**, 92 (2014).
 - ²⁶ D. S. Arnold, A. Tura, A. Ruebsaat-Trott, and A. Rowe, “Design improvements of a permanent magnet active magnetic refrigerator,” *Int. J. Refrig.-Rev. Int. Froid* **37**, 99 (2014).
 - ²⁷ A. Kitanovski, U. Plaznik, U. Tomc, and A. Poredoš, “Present and future caloric refrigeration and heat-pump technologies,” *Int. J. Refrig.-Rev. Int. Froid* **57**, 288 (2015).
 - ²⁸ J. E. Cararo, J. A. Lozano, P. V. Trevizoli, R. Teyber, A. Rowe, and J. R. Barbosa Jr., “Optimization of Active Magnetic Regenerators with two and three layers of Gd and Gd-alloys,” in *Proceedings of the 7th Int. Conf. on Magn. Refrig. at Room Temp. – THERMAG VII* (2016) p. 115.
 - ²⁹ B. Monfared and B. Palm, “A new magnetic refrigeration prototype with application in household and professional refrigerators,” in *Proceedings of the 7th Int. Conf. on Magn. Refrig. at Room Temp. – THERMAG VII* (2016) p. 146.
 - ³⁰ H. N. Bez, K. Navickaite, T. Lei, K. Engelbrecht, A. Barcza, and C. R. H. Bahl, “Epoxy-bonded La(Fe,Mn,Si)₁₃H₂ as a multi layered active magnetic regenerator,” in *Proceedings of the 7th Int. Conf. on Magn. Refrig. at Room Temp. – THERMAG VII* (2016) p. 158.
 - ³¹ F. Scarpa, L. A. Tagliafico, and M. Gigante, “Rotary magnetic regenerator design and assembly,” in *Proceedings of the 7th Int. Conf. on Magn. Refrig. at Room Temp. – THERMAG VII* (2016) p. 303.
 - ³² R. Teyber, P. V. Trevizoli, T. V. Christiaanse, P. Govindappa, I. Niknia, and A. Rowe, “Performance evaluation of two-layer active magnetic regenerators with second-order magnetocaloric materials,” *Appl. Therm. Eng.* **106**, 405 (2016).
 - ³³ M. D. Kuz'min, “Factors limiting the operation frequency of magnetic refrigerators,” *Appl. Phys. Lett.* **90**, 251916 (2007).
 - ³⁴ P.-W. Ma and S. L. Dudarev, “Dynamic magnetocaloric effect in bcc iron and hcp gadolinium,” *Phys. Rev. B* **90**, 024425 (2014).
 - ³⁵ J. D. Moore, K. Morrison, K. G. Sandeman, M. Katter, and L. F. Cohen, “Reducing extrinsic hysteresis in first-order La(Fe,Co,Si)₁₃ magnetocaloric systems,” *Appl. Phys. Lett.* **95**, 252504 (2009).
 - ³⁶ K. Morrison, J. D. Moore, K. G. Sandeman, A. D. Caplin, and L. F. Cohen, “Capturing first- and second-order behavior in magnetocaloric CoMnSi_{0.92}Ge_{0.08},” *Phys. Rev. B* **79**, 134408 (2009).
 - ³⁷ K. Morrison, J. Lyubina, J. D. Moore, A. D. Caplin, K. G. Sandeman, O. Gutfleisch, and L. F. Cohen, “Contributions to the entropy change in melt-spun LaFe_{11.6}Si_{1.4},” *J. Phys. D: Appl. Phys.* **43**, 132001 (2010).
 - ³⁸ K. Morrison, M. Bratko, J. Turcaud, A. Berenov, A. D. Caplin, and L. F. Cohen, “A calorimetric method to detect a weak or distributed latent heat contribution at first order magnetic transitions,” *Rev. Sci. Instrum.* **83**, 033901 (2012).
 - ³⁹ E. Lovell, A. M. Pereira, A. D. Caplin, J. Lyubina, and L. F. Cohen, “Dynamics of the First-Order Metamagnetic Transition in Magnetocaloric La(Fe,Si)₁₃: Reducing Hysteresis,” *Adv. Energy Mater.* **5**, 1401639 (2015).
 - ⁴⁰ E. Lovell, M. Bratko, A. D. Caplin, A. Barcza, M. Katter, L. Ghivelder, and L. F. Cohen, “Magnetic relaxation dynamics driven by the first-order character of magnetocaloric La(Fe,Mn,Si)₁₃,” *Phil. Trans. R. Soc. A* **374**, 20150307 (2016).
 - ⁴¹ O. Gutfleisch, T. Gottschall, M. Fries, D. Benke, I. Radulov, K. P. Skokov, H. Wende, M. Gruner, M. Acet, P. Entel, and M. Farle, “Mastering hysteresis in magnetocaloric materials,” *Phil. Trans. R. Soc. A* **374**, 20150308 (2016).
 - ⁴² L. Ghivelder, G. G. Eslava, R. S. Freitas, G. Leyva, and F. Parisi, “Avalanche-like metamagnetic transition in (LaNd)CaMnO manganites,” *J. Alloy. Compd.* **680**, 494

- (2016).
- ⁴³ H. Yako, S. Fujieda, A. Fujita, and K. Fukamichi, "Influence of demagnetizing effect on the kinetics of the itinerant electron metamagnetic transition in magnetic refrigerant $\text{La}(\text{Fe}_{0.88}\text{Si}_{0.12})_{13}$," *IEEE Trans. Magn.* **47**, 2482 (2011).
 - ⁴⁴ A. Fujita and H. Yako, "Kinetics of thermally induced first-order magnetic transition in $\text{La}(\text{Fe}_{0.88}\text{Si}_{0.12})_{13}$ itinerant electron metamagnet," *J. Alloy. Compd.* **577S**, S48 (2013).
 - ⁴⁵ A. Fujita, T. Kondo, M. Kano, and H. Yako, "Shape-anisotropic heterogeneous nucleation and magnetic Gibbs-Thomson effect in itinerant-electron metamagnetic transition of $\text{La}(\text{Fe}_{0.88}\text{Si}_{0.12})_{13}$ magnetocaloric compound," *Appl. Phys. Lett.* **102**, 041913 (2013).
 - ⁴⁶ M. Kuepferling, C. P. Sasso, and V. Basso, "Rate dependence of the magnetocaloric effect in La-Fe-Si compounds," *EPJ Web of Conf.* **40**, 06010 (2013).
 - ⁴⁷ M. Kuepferling, C. Bennati, F. Laviano, G. Ghigo, and V. Basso, "Dynamics of the magneto structural phase transition in $\text{La}(\text{Fe}_{0.9}\text{Co}_{0.015}\text{Si}_{0.085})_{13}$ observed by magneto-optical imaging," *J. Appl. Phys.* **115**, 17A925 (2014).
 - ⁴⁸ M. Ghorbani Zavareh, C. Salazar Mejía, A. K. Nayak, Y. Skourski, J. Wosnitza, C. Felser, and M. Nicklas, "Direct measurements of the magnetocaloric effect in pulsed magnetic fields: The example of the Heusler alloy $\text{Ni}_{50}\text{Mn}_{35}\text{In}_{15}$," *Appl. Phys. Lett.* **106**, 071904 (2015).
 - ⁴⁹ F. Cugini, G. Porcari, C. Viappiani, L. Caron, A. O. dos Santos, L. P. Cardoso, E. C. Passamani, J. R. C. Proveti, S. Gama, E. Brück, and M. Solzi, "Millisecond direct measurement of the magnetocaloric effect of a Fe_2P -based compound by the mirage effect," *Appl. Phys. Lett.* **108**, 012407 (2016).
 - ⁵⁰ A. M. Aliev, A. B. Batdalov, L. N. Khanov, V. V. Koldov, V. G. Shavrov, I. S. Tereshina, and S. V. Taskaev, "Magnetocaloric effect in some magnetic materials in alternating magnetic fields up to 22 Hz," *J. Alloy. Compd.* **676**, 601 (2016).
 - ⁵¹ W. A. Johnson and R. F. Mehl, "Reaction Kinetics in Processes of Nucleation and Growth," *Trans. Am. Inst. Min. Metall. Eng.* **135**, 416 (1939).
 - ⁵² M. Avrami, "Kinetics of Phase Change. I General Theory," *J. Chem. Phys.* **7**, 1103 (1939).
 - ⁵³ M. Avrami, "Kinetics of Phase Change. II Transformation-Time Relations for Random Distribution of Nuclei," *J. Chem. Phys.* **8**, 212 (1940).
 - ⁵⁴ M. Avrami, "Granulation, Phase Change, and Microstructure. Kinetics of Phase Change. III," *J. Chem. Phys.* **9**, 177 (1941).
 - ⁵⁵ C. Bennati, L. Gozzelino, E. S. Olivetti, and V. Basso, "Heterogeneous nucleation and heat flux avalanches in $\text{La}(\text{Fe},\text{Si})_{13}$ magnetocaloric compounds near the critical point," *Appl. Phys. Lett.* **109**, 231904 (2016).
 - ⁵⁶ L. I. Rubinstein, *The Stefan Problem* (American Mathematical Society, Providence – Rhode Island, 1971).
 - ⁵⁷ V. Alexiades and A. D. Solomon, *Mathematical Modeling of Melting and Freezing Processes* (Hemisphere Publishing Corporation – Taylor & Francis Group, Washington, 1993).
 - ⁵⁸ S. C. Gupta, *The Classical Stefan Problem: Basic concepts, Modelling and Analysis*, 1st ed. (Elsevier Science, Amsterdam, 2003).
 - ⁵⁹ A. Visintin, *Models of Phase Transitions* (Birkhäuser, Boston, 1996).
 - ⁶⁰ H. B. Callen, *THERMODYNAMICS AND AN INTRODUCTION TO THERMOSTATISTICS*, 2nd ed. (John Wiley & Sons, New York, 1985).
 - ⁶¹ M. J. O'Neill, "The Analysis of a Temperature-Controlled Scanning Calorimeter," *Anal. Chem.* **36**, 1238 (1964).
 - ⁶² V. Basso, C. P. Sasso, and M. Kuepferling, "A Peltier cells differential calorimeter with kinetic correction for the measurement of $c_p(H, T)$ and $\Delta s(H, T)$ of magnetocaloric materials," *Rev. Sci. Instrum.* **81**, 113904 (2010).
 - ⁶³ V. Basso, M. Kuepferling, C. Curcio, C. Bennati, A. Barzca, M. Katter, M. Bratko, E. Lovell, J. Turcaud, and L. F. Cohen, "Specific heat and entropy change at the first order phase transition of $\text{La}(\text{Fe-Mn-Si})_{13}$ -H compounds," *J. Appl. Phys.* **118**, 053907 (2015).
 - ⁶⁴ D. S. Fisher, "Scaling and Critical Slowing Down in Random-Field Ising Systems," *Phys. Rev. Lett.* **56**, 416 (1986).
 - ⁶⁵ C. Djurberg, P. Svedlindh, P. Nordblad, M. F. Hansen, F. Bødker, and S. Mørup, "Dynamics of an Interacting Particle System: Evidence of Critical Slowing Down," *Phys. Rev. Lett.* **79**, 5154 (1997).